TECHNICAL REVIEWS

High-resolution neutron spectroscopy using backscattering and neutron spin-echo spectrometers in soft and hard condensed matter

Jason S. Gardner[1]*, *Georg Ehlers*[2], *Antonio Faraone*[3] and *Victoria García Sakai*[4]

Abstract | The instruments best suited to performing high-energy-resolution neutron spectroscopy are spin-echo spectrometers and backscattering spectrometers. The development of these experimental techniques dates back almost half a century, and most major neutron scattering facilities operate mature spectrometers of one or both classes. Recent advances in instrumentation and neutron sources are enhancing their performance and expanding their capabilities, with the objective of enabling researchers to tackle new and more complex problems. In this Technical Review, we assess the current state of the art in high-energy-resolution neutron spectrometers, showcasing their role in the study of nanoscale dynamics in soft and biological materials, as well as disordered magnets.

[1]*Neutron Platform, Songshan Lake Materials Laboratory, Dongguan, China.*

[2]*Neutron Technologies Division, Oak Ridge National Laboratory, Oak Ridge, TN, USA.*

[3]*Center for Neutron Research, National Institute of Standards and Technology, Gaithersburg, MD, USA.*

[4]*ISIS Neutron and Muon Source, Science and Technologies Facilities Council, Rutherford Appleton Laboratory, Didcot, UK.*

**e-mail: jason.gardnerfinstp@gmail.com*

https://doi.org/10.1038/s42254-019-0128-1

The dynamic processes that occur on the nanoscale in many materials, ranging from proteins and quantum magnets to catalysts, are crucial to their functionality and are often essential to understanding their bulk properties. A wide range of characterization tools can be used to probe the complex set of dynamic modes that are found in materials, including dielectric spectroscopy, muon spin spectroscopy, NMR or Mössbauer spectroscopy. However, the scattering of quantum particles or radiation, such as visible light, X-rays or neutrons, provides information on both the timescales and length scales of motion. Among these probes, thermal and cold neutrons have wavelengths and energies on the order of interatomic distances and excitation energies in matter, respectively; thus, neutron spectroscopy is uniquely positioned to study the behaviour in materials on the nanometre length scale and nanosecond timescale[1,2]. In this Technical Review, we focus on neutron spectroscopy, specifically, high-energy-resolution methods, which are used to probe dynamic processes that occur on timescales from picoseconds to hundreds of nanoseconds. High energy resolution is an arbitrary term used by the neutron scattering community, with no exact quantitative definition. In general, this term refers to spectrometers that have an energy resolution in the μeV range, specifically neutron spin-echo (NSE) and backscattering spectrometers. FIGURE 1 shows the temporal and spatial scales that can be accessed using these neutron spectrometers compared with those of more commonly used experimental techniques.

Key aspects of neutron scattering

As neutrons have no charge, they are insensitive to the charge in the electron cloud of atoms and are scattered directly by the nuclei. The interaction potential between a neutron and the nucleus, quantified as a scattering cross section, is isotope dependent[3] (Supplementary Table 1); for example, there is a notable difference in the scattering cross sections of hydrogen and its less-common isotope, deuterium (the incoherent cross sections are $80.26 \times 10^{-28}\,m^2$ and $2.05 \times 10^{-28}\,m^2$ for hydrogen and deuterium, respectively). Thus, neutron scattering is an indispensable tool in the study of time and space correlations in soft matter and biological systems, which are rich in hydrogen atoms. Subsequently, hydrogen–deuterium substitution is commonly used to control the source of the neutron scattering signal to, for example, make certain atoms, molecular structures or system components invisible without (to a first approximation) affecting the sample chemistry. In addition, a neutron also has a spin, which couples to the magnetic moments of a material through a dipolar interaction. This spin–moment coupling makes neutron scattering an irreplaceable probe for magnetism.

The interaction between a neutron and a nucleus is described by the Fermi pseudopotential through a single parameter, the scattering length b, which determines the scattering probability. The scattering potential of an atom depends on its nuclear spin, which is usually disordered. Therefore, there is often a random variation of the scattering lengths of a specific atom, owing to the

Key points

- Neutron scattering is a uniquely powerful experimental method to study the structure and dynamics in materials.
- Neutron spin-echo and backscattering spectrometers probe the dynamics in materials on the picosecond and nanosecond timescales and provide spatial information on the motions over ångström to nanometre length scales.
- High-resolution scattering studies have contributed to a wide range of scientific fields, from nanosized data storage and carbon sequestration to the efficiency of modern batteries and drug delivery systems.
- The state of the art of these instruments is constantly evolving, in particular in improving the resolution and accelerating the rate at which data can be acquired.

random population of different isotopes and the randomness of the nuclear spin direction. This variation enables nuclear neutron scattering to be separated into a so-called coherent component (related to the average scattering length of an element), which provides information on the relative position and motion of different atoms, and an incoherent component (related to the random deviation from the average), which yields information on the single particle dynamics of the atoms. Thus, the coherent and incoherent scattering lengths of an atom are defined by the average of b over all isotopes and spin states and by its root mean square deviation, respectively. The coherent and incoherent scattering cross sections are defined by 4π times the square of the coherent and incoherent lengths, respectively.

Owing to the neutron spin, neutron beams can also be spin polarized, and the polarization can be manipulated by magnetic fields. This capability is used in the spin-echo technique, which is discussed below. Coherent scattering does not alter the spin of the neutron, whereas incoherent scattering (when it originates from a distribution of nuclear magnetic moments rather than the presence of various isotopes) has a 2/3 probability of flipping the neutron spin. As the scattering of a neutron by a magnetic moment depends on the relative orientations of the neutron spin and the wavevector transfer **Q**, controlling the beam polarization in an experiment offers another degree of freedom that is relevant for magnetic neutron scattering.

The interaction of neutrons with matter is relatively weak; thus, neutrons can penetrate through most materials and rarely cause damage or changes to the sample under study (beam heating is rarely an issue at millikelvin temperatures or above). Furthermore, complex and bulky sample environment equipment can surround the sample to enable measurements under various conditions, including tension or shear, very low temperature (millikelvin) or extreme heat (<2,000 °C), high pressure (on the order of gigapascals), high magnetic fields (<26 T) or a combination of these. Unfortunately, neutron scattering methods are limited by the low flux of available neutron beams, and the beams are not easily focused. Therefore, experiments generally require large samples (with a mass in the range of hundreds of milligrams to grams). In addition, a few isotopes are strong neutron absorbers, which poses a problem if one of these isotopes is present in a sample.

Neutron beams are currently produced by either fission reactors or spallation sources. Once a free particle, a neutron passes a moderator volume, which reduces or moderates its energy to that required by a specific instrument. Moderators generally contain light atoms or molecules, such as water or liquid hydrogen. The mean energy of a neutron beam emanating from a room-temperature water moderator is ~25 meV (with a wavelength (λ) of 1.8 Å); hence, neutrons having approximately this energy are termed thermal neutrons. To probe slow dynamics, such as those described in the following, typically requires cold neutrons of less than ~5 meV (with $\lambda \geq 4$ Å) obtained, for example, from a liquid hydrogen moderator. In general, the wavelength dependence of the neutron flux can be described by a Boltzmann distribution that peaks in the 2–4 Å range and decreases at long wavelengths as λ^{-5}.

Neutron spectroscopy. In a traditional neutron scattering experiment[4], the quantity measured is the double differential scattering cross section, where σ is the total scattering cross section (equation 1)

$$\frac{\mathrm{d}^2\sigma}{\mathrm{d}\Omega \mathrm{d}E} \propto \frac{|\mathbf{k}_\mathrm{s}|}{|\mathbf{k}_\mathrm{i}|} S(\mathbf{Q}, E) \qquad (1)$$

which is the probability that the neutron is scattered in the solid angle, $\mathrm{d}\Omega$, and exchanges an energy, $E = E_\mathrm{s} - E_\mathrm{i} = (\hbar\mathbf{k}_\mathrm{s})^2/2m_\mathrm{n} - (\hbar\mathbf{k}_\mathrm{i})^2/2m_\mathrm{n}$, and a momentum $\hbar\mathbf{Q} = \hbar\mathbf{k}_\mathrm{s} - \hbar\mathbf{k}_\mathrm{i}$, with the sample. Here, $\hbar$ is the reduced Planck's constant; m_n is the neutron mass; $\mathbf{k}_\mathrm{s}$ and $\mathbf{k}_\mathrm{i}$ are the wavevectors of the scattered and incoming neutron, respectively; and E_s and E_i are the energies of the scattered and incoming neutron, respectively. In the energy range of usual high-energy-resolution neutron spectrometers, $|\mathbf{k}_\mathrm{i}| = |\mathbf{k}_\mathrm{s}| = 2\pi/\lambda$ and $|\mathbf{Q}| = Q = (4\pi/\lambda)\sin\theta$, which relates the magnitude of the wavevector transfer, Q, to the neutron wavelength, λ, and the scattering angle, 2θ.

According to the well-established van Hove picture[5], the dynamic structure factor $S(\mathbf{Q},E)$ is the time and space Fourier transform of the two-point correlation function between the atomic positions in the sample (equation 2)

$$S(\mathbf{Q}, E) = \int_{-\infty}^{\infty} \sum_{\mathrm{i,j}} \langle b_\mathrm{i} b_\mathrm{j} \exp\{i\mathbf{Q}[\mathbf{r}_\mathrm{i}(t) - \mathbf{r}_\mathrm{j}(0)]\}\rangle \exp\left(-i\frac{Et}{\hbar}\right)\mathrm{d}t \qquad (2)$$

where b_i and b_j, and $\mathbf{r}_\mathrm{i}$ and $\mathbf{r}_\mathrm{j}$ are the neutron scattering lengths and positions of atoms i and j, respectively. A similar equation can be written for the magnetic scattering from unpaired electrons[2]. Equation 2 demonstrates the inverse relationship between **Q** and distance (or length scale) and between E and time (t), implying that better energy resolution enables the study of slower dynamic processes.

If only spatial correlations are of interest, measurements are taken using diffractometers, with which no energy analysis of the scattered neutrons is performed (essentially, $S(\mathbf{Q},E)$ is integrated over E). However, to probe dynamic modes in a sample, it is necessary to use a neutron spectrometer that measures the energy transfer E.

Coherent scattering
Wavevector transfer (Q)-dependent scattering that contains information about scattering structures.

Incoherent scattering
Relatively weakly wavevector transfer (Q)-dependent scattering that contains information about the movement of an individual atom in time.

Fission
A nuclear reaction in which a massive nucleus splits into smaller nuclei with the simultaneous release of energy, neutrons and other products.

Spallation
A process by which a heavy nucleus ejects smaller particles, including neutrons, after, for example, being hit with high-energy particles.

Moderator
A material used to reduce the energy of free neutrons by a large number of inelastic collisions.

Thermal neutrons
Unbound or free neutrons with an average energy of ~25 meV at room temperature.

Cold neutrons
Unbound or free neutrons with an average energy lower than ~5 meV.

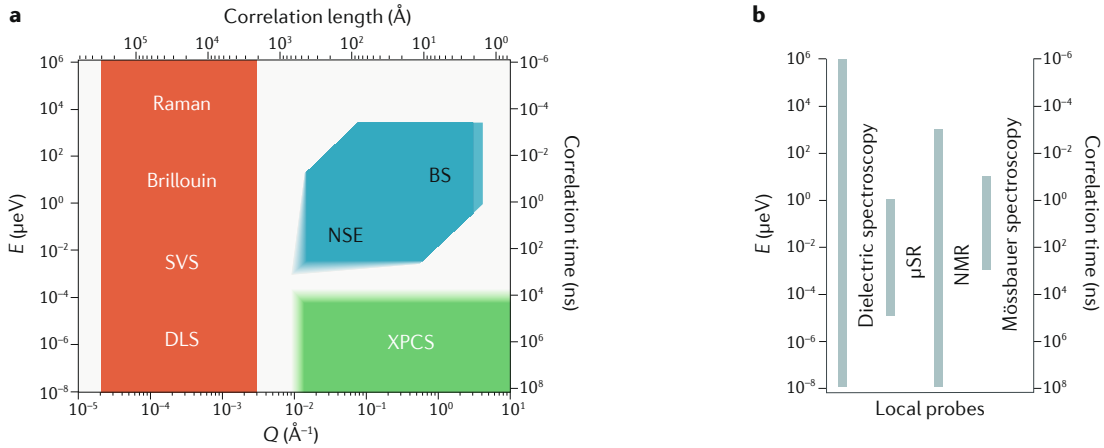

Fig. 1 | **Timescales and length scales probed by different experimental techniques. a** | High-energy-resolution neutron spectrometers, such as neutron spin-echo (NSE, light blue) and backscattering (BS, dark blue) spectrometers, cover the nanometre and nanosecond range. The orange area corresponds to visible light techniques, including Raman spectroscopy, Brillouin spectroscopy, speckle visibility spectroscopy (SVS) and dynamic light scattering (DLS). The boundaries of the various techniques are not sharp as they partially depend on the characteristics of the samples. Moreover, all techniques are continuously pushing their boundaries, in some cases progressing rapidly, as in the case of X-ray photon correlation spectroscopy (XPCS, green) with the development of more coherent and brighter sources and detector technology. **b** | Comparison of local probes. Energy (E) is defined as $\hbar$/timescale (where $\hbar$ is the reduced Planck's constant) and the wavevector transfer (Q) as 2π/length scale, where $\hbar Q$ is the momentum transfer. μSR, muon spin relaxation.

In materials, motions can be broadly characterized as either excitations that take place at a defined energy transfer E (observed as a distinct peak intensity in $S(\mathbf{Q},E)$), for which there is an inherent restoring force, such as periodic natural modes (phonons or magnons) or vibrational modes; or as a relaxation, for which there is no restoring force and the inherent dynamics are diffusive in nature. In the latter case, the observed scattering signal appears as a broadening of the so-called elastic line, which is referred to as quasi-elastic neutron scattering (QENS). QENS is the main measurement associated with the instruments discussed herein. The elastic line represents zero energy transfer, where 'zero' is the smallest energy transfer that can be measured by a given spectrometer and is also referred to as the energy resolution of the instrument. The elastic line contains information on motions that are too slow to be measured. In general, any spectrometer can be used to probe vibrational or relaxational dynamics; however, because of the typical energy scales involved, vibrations are most commonly studied on instruments with energy resolutions of the order of meVs, such as three-axis, direct-geometry or vibrational neutron spectrometers. The diffusional and transport processes that occur in biological and liquid-based systems, relaxations in polymers and colloidal systems, interfacial fluctuations in complex fluids, and relaxation phenomena in both structural and spin glasses as well as frustrated magnets all occur at slower timescales (tens of picoseconds to hundreds of nanoseconds). To probe such relaxational dynamics, spectrometers with a μeV energy resolution (that is, a high energy resolution), such as backscattering and NSE are needed.

In the following, we discuss, in turn, the fundamental principles of NSE and backscattering instruments, the current status and recent advances in technology, and future directions for their development. We then showcase the applicability of these techniques to study relaxations at the nanoscale using examples from the fields of soft and hard condensed matter, specifically polymer science, biophysics and magnetism. However, the scientific questions that can be addressed using this technique go well beyond these systems and include, among others, diffusion in liquids, conduction in energy-relevant and functional materials, and diffusion in solids, such as catalysts. A broader overview of the scientific opportunities offered by these techniques can be found elsewhere[6–9].

Neutron spin-echo spectrometers

NSE spectrometers provide the highest energy resolution of all neutron spectroscopy techniques. Of the currently operational instruments (TABLE 1), IN15 at the Institut Laue–Langevin (ILL; France)[10] offers the highest resolution of ~1 neV. This means that IN15 can probe dynamic processes with characteristic times of up to almost a microsecond, thus making it the ideal technique to observe slow relaxations in polymers (such as reptation), dynamics such as bending in amphiphilic membranes and fluctuations in soft colloidal systems or normal modes in proteins in solution. In hard matter, it is used to probe spin glasses, critical magnetic fluctuations or emergent excitations in quantum magnetism.

In the NSE technique, the velocity changes experienced by the neutrons as they interact with matter are determined by measuring the change in the Larmor precession of their spins in a magnetic field (BOX 1). NSE spectrometers are commonly, and most efficiently, employed to measure the motions of nanosized structures, such as polymers, proteins and self-assembled complexes; however, measurements on molecular liquids and solid materials are also performed to investigate structural relaxations, the single particle dynamics of hydrogen atoms or spin dynamics.

Table 1 | **Characteristics of current neutron spin-echo spectrometers**

Name	Facility	Type	Unique features	Q range (Å^{-1})	Max. t_F (ns)	Ref.
IN15	ILL	Mezei with a ToF option	Low Q, high energy resolution	0.001–2.0	1,000	10
IN11	ILL	Mezei	–	0.02–2.7	50	155
WASP	ILL	Mezei with an anti-Helmholtz coil	Wide angle, high Q	0.03–3.0	50	19
J-NSE-Phoenix	FRM II	Mezei	–	0.01–1.7	500	16
NSE	SNS-ORNL	ToF Mezei	ToF, high Q	0.03–4.0	100	11
CHRNS-NSE	NCNR	Mezei	–	0.02–1.7	100	156
MUSES	LLB	Resonance	High Q	0.03–2.9	22	157
RESEDA	FRM II	Resonance	High-Q magnetism	<2.5	20	13
iNSE	JRR-3	Mezei	–	0.03–2.8	50	158
VIN ROSE	J-PARC	MIEZE	Low-Q magnetism	Commissioning		12
VIN ROSE	J-PARC	Resonance	High Q	Commissioning		12

The accessible wavevector transfer (Q) range and the maximum Fourier time (t_F) depend on the incident beam conditions. CHRNS, Center for High Resolution Neutron Scattering; FRM II, Forschungs-Neutronenquelle Heinz Maier-Leibnitz; ILL, Institut Laue–Langevin; J-NSE, Jülich-neutron spin-echo; J-PARC, Japan Proton Accelerator Research Complex; JRR-3, Japan Research Reactor-3; LLB, Laboratoire Léon Brillouin; MIEZE, modulation of intensity by zero effort; NCNR, National Institute of Standards and Technology (NIST) Center for Neutron Research; NSE, neutron spin echo; RESEDA, Resonance Spin Echo for Diverse Applications; SNS-ORNL, Spallation Neutron Source at Oak Ridge National Laboratory; ToF, time of flight; VIN ROSE, Village of Neutron Resonance Spin Echo spectrometers; WASP, wide angle spin-echo spectrometer.

Traditionally, NSE spectrometers have been located at neutron research reactors (TABLE 1) and most are of the traditional Mezei type (Mezei NSE). The first time-of-flight NSE spectrometer, and the only Mezei-type instrument operating at a pulsed source, was built at the Spallation Neutron Source (SNS) at the Oak Ridge National Laboratory (ORNL; United States)[11]. This spectrometer was also the first to employ superconducting precession coils. Currently, two new NSE spectrometers are being developed at the pulsed source in the Material and Life Science (MLF) Experimental Facility at the Japan Proton Accelerator Research Complex (J-PARC)[12]. One of these is a modulation of intensity by zero effort (MIEZE) instrument, which enables measurements on samples that cause a depolarization of the neutron beam, such as ferromagnets and superconductors, which cannot easily be accomplished using classical Mezei-type instruments. A similar MIEZE instrument is available at the Resonance Spin Echo for Diverse Applications (RESEDA) at Forschungs-Neutronenquelle Heinz Maier-Leibnitz (FRM II; Garching, Germany), which also offers a longitudinal resonance spin-echo option[13].

The most important area of technical development in NSE spectrometers concerns the design of the precession coils and correction elements to improve the homogeneity of the field integral, which determines the upper limit of the Fourier times that can be probed. With modern precession coils, it is possible to come close to the theoretical limit of ~200 ppm (REF.[14]), and the inhomogeneity can be further reduced by a factor of ~300 through the use of state-of-the-art correction elements (known as Pythagoras coils)[14]. Recent upgrades of IN15 (REF.[15]) have produced a maximum field integral of 1.2 Tm, which is four times larger than what was previously available on that spectrometer. In combination with the high flux and long wavelength available to IN15, Fourier times of ~600 ns (REF.[10]) can routinely be achieved, and it is even possible, under favourable experimental conditions, to reach 1 μs. A similar performance has been achieved with the superconducting precession coils at the Jülich-neutron spin-echo (J-NSE)-Phoenix instrument at FRM II[16]. This instrument can reach a maximum field integral of 1.5 Tm, and preliminary results indicate a successful reduction of the field inhomogeneities by a factor 2.5 compared with the previous design. With this field integral, the J-NSE-Phoenix spectrometer can reach ~500 ns with 17 Å neutrons[16].

In addition to the improvements in energy resolution, considerable effort has been made to widen the detection area of NSE instruments. Typical Mezei-type instruments have a detector with an area of ~1,000 cm^2, which covers a scattering angle range of ~5° (in comparison, in a typical backscattering spectrometer, >1 steradian is covered with an analyser crystal). This area is appropriate when the signal of interest is concentrated in a small region of the Q space, such as a small-angle neutron scattering pattern, but not when the neutron signal is spread uniformly over Q, such as is the case for incoherent dynamics or in some cases for magnetic spin dynamics (paramagnetic scattering). This desire to perform simultaneous measurements in a large detector has led to the development of a 30° wide detection option for the IN11 instrument[17], which has been successful despite the consequent limitation on the attainable Fourier time. In a further development to reach detection coverage as high as 180° in the Q plane, anti-Helmholtz coils were first employed on SPAN at the Hahn-Meitner Institute (Berlin, Germany)[18], and eventually led to the construction of the WASP (wide angle spin-echo spectrometer) at the ILL[19], which is currently under commissioning. On WASP, the detector coverage is 150° (in the scattering plane) × 2.5° (in the vertical direction) and the maximum field integral is 0.27 Tm, which provides a maximum Fourier time of 10 ns at 6 Å. Covering more than three orders of magnitude in time, WASP is an extremely promising tool for the investigation of slow dynamics over a wide Q range.

Mezei NSE
A type of neutron spin-echo (NSE) spectrometer in which the velocity of each neutron is encoded in its Larmor precession in a magnetic field.

Time of flight
A technique by which the time taken for a neutron to travel a known distance is used to determine its velocity (and thus energy).

Modulation of intensity by zero effort
(MIEZE). A modified resonance neutron spin-echo technique that enables measurements to be taken under conditions that depolarize the neutron beam.

Anti-Helmholtz coils
A pair of coils in which the electrical current flows in opposite directions in the two coils, producing a high-magnetic-field gradient from the centre out.

Box 1 | **Fundamentals of the neutron spin-echo technique**

The neutron spin-echo (NSE) technique[151] is based on the use of Larmor precession to measure small changes in the neutron velocity (1:10^6) after interacting with the sample by observing changes in the beam polarization. A $\pi/2$ flipper rotates the neutron spin, from the neutron velocity direction to the plane perpendicular to the precession field, at the beginning of the instrument to start the precession, and a second flipper rotates the spin in the opposite direction to stop the precession, before the neutron spin direction is analysed.

In a Mezei-type NSE spectrometer (see the figure), the Larmor precession is induced by two magnetic fields of the same intensity on either side of the sample (before and after scattering). Alternatively, the neutron velocity can be encoded in the spin by using radio-frequency flippers. Such resonance NSE spectrometers access shorter dynamic scales than traditional spectrometers and are not discussed further here. In both cases, a π flipper is used to flip the neutron spin around an axis perpendicular to the neutron velocity direction near the sample. If the scattering is purely elastic and there is no change in velocity, the neutrons do not acquire a net precession; at the end of their path through the second arm of the spectrometer, the full beam polarization is recovered at the spin analyser. The full recovery of the initial neutron spin state holds true irrespective of the initial neutron velocity. By contrast, if the velocity changes at the sample, the precession angles in the primary and secondary flight paths will differ and a loss in polarization is observed at the detector, with the loss proportional to the exchanged energy.

Given the velocity spread of the incident beam (defined by choppers on a pulsed source or a velocity selector on a continuous source; both components are shown in the figure but are not used in conjunction), a sinusoidal oscillation of intensity (the echo) is observed when trying to match the precession fields using the phase coil. The amplitude of the echo is proportional to the cosine Fourier transform of the scattering function $S(\mathbf{Q},E)$ (where E is energy and $\mathbf{Q}$ is the wavevector transfer) and is known as the intermediate scattering function, $I(\mathbf{Q},t_F)$ (where t_F is the Fourier time). Data are normalized to the result of a polarized diffraction measurement (which is a static measurement with no energy analysis, corresponding to $\int S(\mathbf{Q},E)dE = I(\mathbf{Q},t_F=0)$ to give $I(\mathbf{Q},t_F)/I(\mathbf{Q},0)$). As the measurement is performed directly in the time domain, the resolution of the instrument can be removed in the data analysis by dividing by an equivalent dataset obtained with a static reference sample. The Fourier time is controlled by the strength of the precession field (the field integral $J = \int_l B dl$ (where B is the magnetic field) along the flight path, l) and the third power of the wavelength (λ); thus, a substantially higher resolution is obtained at longer wavelengths. Ultimately, the energy resolution is set by the highest magnetic field achievable with sufficient homogeneity and the longest neutron wavelength but not by the degree to which the neutron beam is monochromatic[151,152]. Current spectrometers achieve a relative energy resolution, with respect to the energy of the incoming neutrons, of the order of 10^{-6} by using a broad incoming wavelength band ($\Delta\lambda/\lambda$ between 10 and 20%). Image courtesy of Oak Ridge National Laboratory.

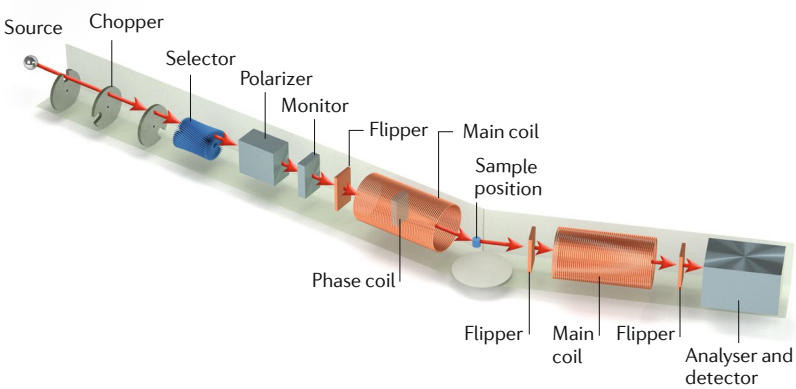

Flipper
A device used to manipulate the neutron spin direction non-adiabatically.

Backscattering spectrometers

Backscattering spectrometers[9] (BOX 2) have a slightly coarser energy resolution than those of NSE spectrometers, achieving a resolution on the order of μeVs, and in contrast to NSE instruments, use unpolarized neutron beams. The information on the dynamic processes accessed by backscattering spectrometers is complementary to that probed using NSE instruments, but with an upper timescale limit of ~10 ns. Thus, backscattering instruments are suitable for probing relaxations in glass-forming systems (such as alpha and beta relaxations), dynamic signatures of phase transitions, molecular reorientations and rotational tunnelling, diffusion in bulk and confined liquids, as well as diffusion in proteins. In general, these instruments are most commonly used to measure the incoherent scattering signal from hydrogenated materials to determine the single particle dynamics of the hydrogen atoms in the sample.

Neutron backscattering spectrometers (BOX 2) use crystals in a perfect (or near-perfect) backscattering geometry (that is, a Bragg angle of 90°) to analyse the scattered neutron energy. TABLE 2 highlights current backscattering instruments and their key characteristics.

Traditional backscattering spectrometers are based on 'strained' Si(111) crystals (for which the Bragg condition is satisfied at $\lambda = 6.27$ Å), offering an energy resolution of the order of ~1 μeV. Currently, the highest-resolution backscattering spectrometer in operation is IN16B at the ILL, which has an energy resolution of ~0.3 μeV, achieved using polished Si(111) crystals[20]. However, as IN16B with polished Si(111) suffers from an order of magnitude loss in intensity, the most commonly used setup uses strained crystals to give an energy resolution of ~0.75 μeV. IN16B also has the option of using strained Si(311) crystals that effectively double the width of the resolution and the dynamic range with only a slight reduction in intensity and also increase the maximum accessible Q from 1.8 $Å^{-1}$ to 3.8 $Å^{-1}$. This increase is of importance when fitting the data to obtain information on the geometry of the motions being probed. An even larger Q range is obtainable by using CaF_2(422) crystals to analyse neutrons with a wavelength of 2.23 Å, as on the IN13 instrument[21]. IN13 therefore provides an unparalleled extended Q range of 0.2–4.9 $Å^{-1}$, but with a coarser energy resolution of ~8 μeV than that acheiveable with Si(111).

The newest additions to the worldwide suite of Si(111)-based backscattering spectrometers are found at spallation sources rather than reactors: the backscattering silicon spectrometer (BASIS at SNS-ORNL)[22] and the biomolecular dynamics spectrometer (DNA at MLF, J-PARC)[12]. Previously, backscattering instruments at pulsed sources were based on pyrolytic graphite, namely IRIS[23] and OSIRIS[24] at the ISIS Neutron and Muon Facility (United Kingdom), which due to a combination of primary and secondary spectrometer design characteristics are limited to a coarser resolution of ~20 μeV (but offer a wider dynamic range and higher intensity). IRIS introduced mica as an analyser to improve the energy resolution but at the high expense of intensity. Si(111) offers a better resolution (for example, achieving an energy resolution of 3.5 μeV) but requires an increased primary flight path length (for example, 84 m for BASIS compared with 36 m for IRIS). Further gains in resolution have been achieved by researchers at DNA by using a pulse-shaping chopper.

More recently, a so-called backscattering and time-of-flight spectrometer (BATS) option has been realized on IN16B[25]; this setup keeps the Si(111) analyser but adds a time-of-flight option to extend the energy window to ±340 μeV with only a slight coarsening of the resolution to 1.2 μeV. This was a highly innovative upgrade,

Box 2 | **Fundamentals of backscattering spectrometers**

The energy of the detected scattered neutrons are fixed using Bragg reflection from an analyser crystal (see the figure). The scattering intensity as a function of energy (E) is determined by scanning the energy of the incoming neutrons. Backscattering spectrometers work on the principle of using crystal analysers at a Bragg angle of 90°. This condition is obtained through differentiation of Bragg's Law: from $\lambda = 2d\sin\theta$ (where λ is the wavelength, d is the interplanar distance and θ is the scattering angle), one obtains $\Delta E/2E = \Delta\lambda/\lambda = \Delta d/d + \cot\theta\Delta\theta$, such that at the exact backscattering condition, the only contribution to the energy resolution is $\Delta d/d$. Under this condition, the wavelength band, $\Delta\lambda$, becomes very narrow as it depends on the crystal properties (such as lattice strain and extinction terms) only and not on the beam divergence. Changing the crystal type therefore changes the energy resolution. A set of choppers (at a pulsed source) or a neutron-velocity selector and a Doppler monochromator (at a reactor source) define the incoming neutron wavelength band. Both components are shown in the figure but are not used in conjunction. An alternative to a Doppler drive is to scan the incident neutron energy by thermal expansion of the crystals (as is done on IN13 at the Institut Laue–Langevin). At reactors, a phase-space transformation (PST) chopper is used to modify the distribution of the incoming neutron momentum to match the resolution of the primary and secondary spectrometer and substantially increase the incoming flux.

Most backscattering spectrometers at reactor sources use a Si(111) analyser crystal array that covers a wavevector transfer, Q, (or angular) range of ~0.2–1.8 Å^{-1}. The Doppler monochromater shifts the incoming neutron wavelength to provide an energy range of approximately ±30 μeV, equivalent to a single order of magnitude in time. Different values of $\Delta d/d$ can be used to modify the energy resolution and the dynamic range (in addition to the Q range).

At pulsed sources, most backscattering spectrometers operate on the same underlying principle as that of reactor sources, but the freedom to select an incoming wavelength by neutron time of flight expands the dynamic range. Here, the energy resolution (ΔE) depends not only on the crystal properties and the Bragg angle of the analyser (that is, the contribution from the secondary spectrometer, ΔE_s) but also on the contribution from the primary spectrometer (ΔE_p; timing and flight path uncertainties), in this case $\Delta E = (\Delta E_p^{\,2} + \Delta E_s^{\,2})^{1/2}$. A well-designed spectrometer matches the characteristics of the primary and secondary spectrometers. In practice, this usually means coarsening the high resolution of the secondary spectrometer to avoid reductions in the dynamic range or intensity. Thus, the spectrometers are typically built in near-backscattering, slightly off a 90° Bragg angle; for example, 88° on the BASIS spectrometer at the Spallation Neutron Source at the Oak Ridge National Laboratory[22] and 87.5° on IRIS at the ISIS Neutron and Muon Facility[22]. Despite pulsed backscattering instruments having a slightly coarser energy resolution than those at reactors, they access a considerably larger dynamic range (approximately hundreds of μeV), providing access to three orders of magnitude in relaxation times. Image courtesy of Oak Ridge National Laboratory.

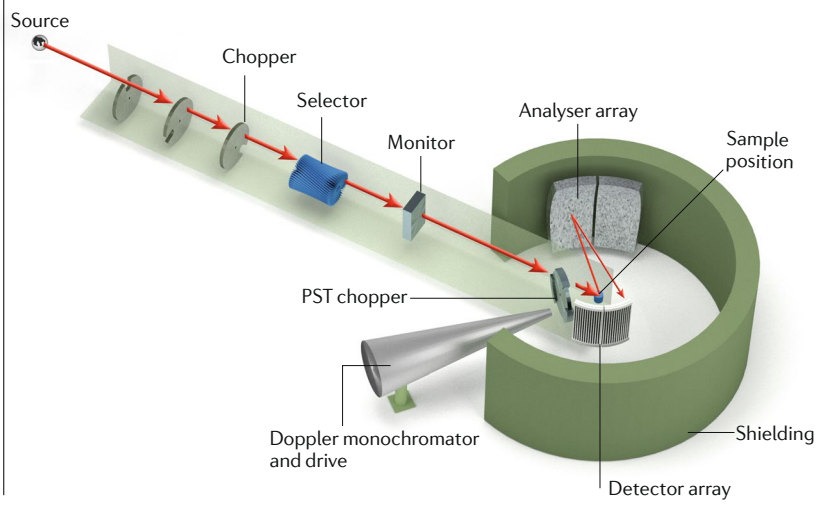

requiring technological progress in chopper disk construction, which has increased the flexibility of the operation of the instrument, enabling new scientific challenges to be addressed, such as the study of more complex systems with dynamics that span many decades.

Dynamics in soft and biological matter

High-energy-resolution neutron spectrometers provide unique information relevant to understanding the dynamics in soft matter and biophysics research, for example, in addressing structure–dynamics–function relationships in proteins, transport processes in membranes (biological or synthetic) and in the design of new polymeric materials with controlled, tunable and 'smart' properties. As most biological and soft matter materials are rich in hydrogen, isotopic substitution (primarily between hydrogen and deuterium) is a powerful approach to study the dynamics of a specific part of a molecule or a component in a multicomponent system[5,10,26,27]. Furthermore, separation of the neutron–sample interaction into coherent and incoherent scattering provides additional information about structurally relevant dynamics and cooperative motions. Measurements on backscattering and NSE spectrometers are ideally suited to probe many of the dynamic modes and relaxation processes that occur in soft materials and biological molecules, from the very local and fast rotations or vibrations that are essential precursors to the slower and larger-scale chain dynamics or diffusional processes that determine macroscopic behaviour.

Polymers. Polymer relaxations have been studied with high-resolution neutron spectroscopy for at least 50 years[5,7,28,29], resulting in well-established relaxation maps for, at least, linear homopolymers. Since the 2000s, interest in more complex polymer-based systems, such as polymer electrolytes[30], polymers of complex architectures (for example, dendrimers)[31], mixtures of two or more polymers (blends)[32] or mixtures with hard[33–35] or soft[36,37] components (nanocomposites), and associating polymers[38], has been driven primarily by the interest in possible applications. In these systems, the underlying molecular dynamics and the relationship with the macroscopic, that is, rheological behaviour, is still not fully understood. These more complex systems exhibit fundamental features of interest, such as surface, confinement and nanostructuring effects[39]. In polymer nanocomposites, for example, high-energy-resolution neutron spectroscopy measurements have shown that the dynamics of polymer chains at the surface of nanoparticles with attractive interactions with the polymer are not frozen. However, the translational dynamics of the chains is suppressed and the Rouse dynamics altered[40], in agreement with results from confined polymer chains[39,40]. In addition, measurements have also highlighted the existence of two competing effects on the reptation tubes of polymers in polymer nanocomposites[33]: tube dilation due to chain disentanglement and a reduction in the reptation tube owing to geometrical confinement, the latter contribution being dominant for nanoparticle volume fractions of more than ~35% (REF.[41]). As revealed by NSE measurements, the dilation of the reptation tube can explain the anomalous softening of some polymer nanocomposites. The dilation can originate from, for example, the disentangling of polymer chains in nanocomposites with dynamically asymmetric polymers[35,37]; here, dynamical asymmetry refers to the interplay between a polymer with a high glass transition temperature (T_g), such as poly(methylmethacrylate), and a polymer with a low T_g,

Table 2 | **Characteristics of current backscattering spectrometers**

Name	Facility	Crystals	Resolution (μeV)	Dynamic range (μeV)	Q range ($Å^{-1}$)	Ref.
IN16B	ILL	Si(111) polished	~0.3	±31	0.1–1.8	20
IN16B	ILL	Si(111) strained	~0.75	±31	0.1–1.8	20
IN16B	ILL	Si(311) strained	~2.0	±59	0.7–3.8	20
IN13	ILL	CaF_2(422)	~8.0	±200	0.2–4.9	21
SPHERES	FRM II	Si(111) strained	~0.65	±31	0.2–1.8	159
EMU	ANSTO	Si(111) strained	~0.9	±32	0.01–2.0	160
HFBS	NCNR	Si(111) strained	~0.9	±35	0.2–1.8	161
BASIS	SNS-ORNL	Si(111)	3.5	$\pm10^2$	0.2–2.0	22
BASIS	SNS-ORNL	Si(311)	15	$\pm10^3$	0.4–3.8	22
IRIS	ISIS	Pyrolytic graphite (002)	17.5	$\pm5.5\times10^2$	0.44–1.85	23
IRIS	ISIS	Pyrolytic graphite (004)	54.5	$\pm3.5\times10^3$	0.89–3.71	23
IRIS	ISIS	fMica (002)[a]	1.2	$\pm2\times10^1$	0.12–0.62	23
IRIS	ISIS	mMica (004)	4.5	$\pm2\times10^2$	0.24–1.24	23
OSIRIS	ISIS	Pyrolytic graphite (002)	24.5	$\pm6\times10^2$	0.18–1.8	24
OSIRIS	ISIS	Pyrolytic graphite (004)	100	$\pm3.5\times10^3$	0.37–3.6	24
DNA	J-PARC	Si(111)	2.4	$\pm10^2$	0.08–1.98	12
DNA	J-PARC	Si(311)[b]	7.6	$\pm10^2$	1.04–3.79	12

Owing to the different configurations, there are multiple entries for a single instrument. ANSTO, Australian Nuclear Science and Technology Organization; BASIS, backscattering silicon spectrometer; FRM II, Forschungs-Neutronenquelle Heinz Maier-Leibnitz; HFBS, high-flux backscattering spectrometer; ILL, Institut Laue–Langevin; J-PARC, Japan Proton Accelerator Research Complex; NCNR, National Institute of Standards and Technology (NIST) Center for Neutron Research; SPHERES, spectrometer for high energy resolution; SNS-ORNL, Spallation Neutron Source at Oak Ridge National Laboratory. [a]Fluorinated mica (fMica) provides a higher signal-to-noise ratio than that of muscovite mica (mMica). [b]Under planning.

such as poly(ethylene oxide). A similar dilation of the reptation tube has also been observed in athermal polymer nanocomposites (systems in which the net enthalpic interactions between the surface of the nanoparticles and the polymer chains are negligible, that is, neither attractive nor repulsive) when the size of the nanoparticles is smaller than the entanglement mesh size[42]. This study provides a straightforward example of the microscopic insight neutron scattering techniques can provide in the study of polymer composite materials and therefore the main neutron data are reported in FIG. 2 to demonstrate typical experimental results.

Proteins. Proteins are multiscale entities and their dynamics occur over several decades, from the atomic to the macroscopic scale. High-resolution neutron spectroscopy provides key insight into the dynamics of these systems at the atomic and molecular level. Over the ångström length scale at timescales shorter than a nanosecond, and following the seminal work of Doster and co-workers[43], much work has been devoted to investigating the so-called dynamical transition (T_d) in protein powders, its relationship with the dynamics of the solvent and its connection to the onset of protein function[44]. Studies have mainly focused on probing the onset of anharmonic motions and the relationship between these motions and the onset of biological activity using simple globular and model proteins. The effect of external parameters, such as pressure, temperature and salt concentration, provides insight into biological adaptation to extreme environments[45]. For example, the adaptive properties of extremophiles remain mysterious, but using neutron spectroscopy, three behaviours have been observed: reduced internal dynamics at high pressure, especially above T_d, resulting from a roughening of the energy landscape[46]; stabilizing effects of high salt concentrations on the hydrogen-bonding network in halophiles without penetration into the biomass[47]; and an entropic argument to explain the increased flexibility in the folded state of thermophiles compared with that of their mesophilic counterparts[48]. Although much work continues to be done on simple or model proteins, researchers are successfully extending their investigations using backscattering spectrometers, in particular, to more biologically relevant systems by studying complex structures such as cancer cells[49] or neural tissues[50].

At longer length scales, on the order of several nanometres, the motions of large domains are fundamental to the function of proteins as biological machines, enabling molecular groups to reach the required proximity or co-enzymes to access the catalytic sites. Knowledge of these dynamics could be crucial for the design of new drugs. To this end, unique experimental information can be obtained using NSE spectrometers owing to their nanoscale space–time sensitivity and the possibility of probing, through the coherent neutron signal, the conformational dynamics of proteins (that is, the motion of one domain relative to another)[17]. Such studies have highlighted how large domain motions are overdamped (relaxational) movements and can often be described in terms of normal modes. In addition, it is possible to extract information on the friction experienced by the domains and/or the elastic constant[51] of the flexible linker. NSE measurements can also be performed

Resonance NSE spectrometers
A type of neutron spin-echo (NSE) spectrometer that employs radio-frequency spin flippers to manipulate the spin of each neutron and encode its velocity.

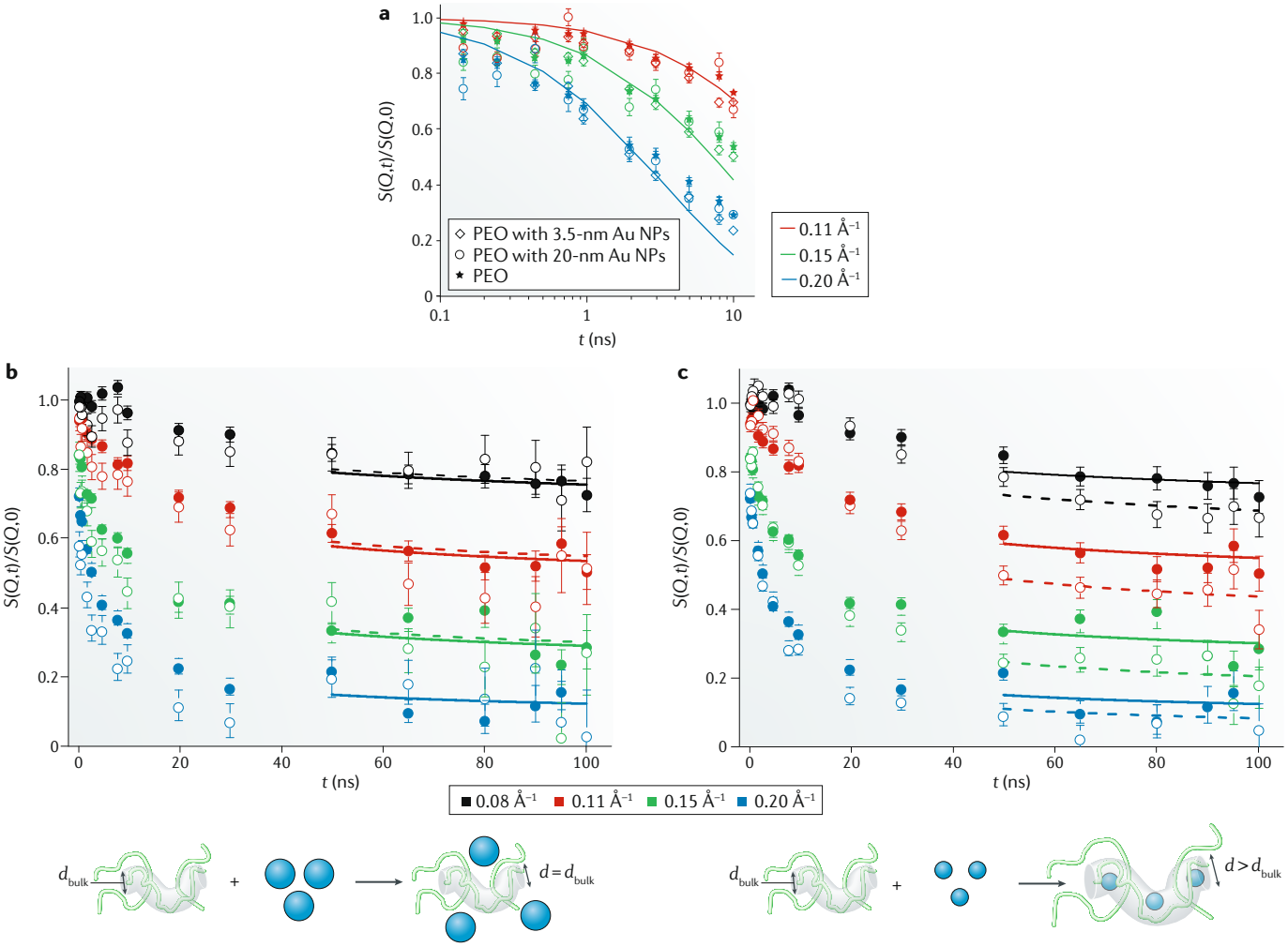

Fig. 2 | **Measuring chain dynamics in polymer nanocomposites.** Neutron spin-echo spectroscopy has been used to probe the chain dynamics in entangled poly(ethylene oxide) (PEO) with a molecular weight (M_w) of 35,000, with and without gold (Au) nanoparticles coated with a thin 'corona' of short (M_w = 600) PEO chains[42]. The normalized intermediate scattering functions, here denoted as $S(Q,t)/S(Q,0)$ (where Q is the wavevector transfer) are plotted as a function of time (t) for neat PEO (filled symbols) and PEO nanocomposites with Au nanoparticles (NPs) of different sizes (small NPs of 3.5 nm and large NPs of 20.2 nm; open symbols) at 400 K. **a** | At short times (t < 10 ns), the initial Rouse decays are identical for neat PEO and for the two nanocomposites, indicating that in these systems the segmental dynamics remains unchanged. The lines are the Rouse model predictions[153]. **b** | For the nanocomposite with large NPs, the long-time plateau is identical to that of neat PEO (top part), which implies that the size of the reptation tube diameter, d, is not changed with respect to the one of bulk PEO, d_{bulk} (bottom part). **c** | For the nanocomposite with small NPs, the long-time decay decreases with respect to that of neat PEO (top part), which is indicative of dilation of the diameter of the reptation tube (bottom part). The lines in panels **b** and **c** are the global fits to results from the de Gennes equation[154] using the elementary Rouse rate reported in REF.[153]. The size of the reptation tube diameter is determined from the Q dependence of the plateau height. Error bars are calculated from the counting statistics of the spin-echo measurement. Adapted with permission from REF.[42], American Physical Society.

on intrinsically disordered[52] or denaturated proteins[53], revealing whether polymer-like models apply. The methods and recent results on internal protein dynamics have been reviewed elsewhere[54,55]. Despite the relevance of these studies, access to protein domain motions with the NSE technique is limited by several practical difficulties: the size of the protein and its domain need to be such to provide a sufficient signal; a relatively large amount of protein is required; and the analysis of the data to disentangle the conformational dynamics from other processes, such as diffusion and rotation as well as inter-particle interactions, is often complex and might benefit from the use of molecular dynamics simulations[56]. Combining NSE data with that from backscattering experiments can offer some help if, for example, the data is for perdeuterated protein powders; without solvent, the global motion of the protein molecules is suppressed, thereby enabling a clearer characterization of the collective internal dynamics. Observed collective motions on the 100 ps timescale are pathways for the larger-scale domain motions that are accessible with NSE[57] in protein solutions as indicated by results from molecular dynamics simulations, which are in good agreement with the experimental data. Another example of the study of the collective motions of proteins[58] in the subnanosecond timescale involved the careful

analysis of QENS data from human deoxy-haemoglobin and CO-bound haemoglobin in solution, revealing that although the deoxy-haemoglobin performs simple translational and rotational rigid-body movements, the CO-bound form exhibits additional large-scale motions that result from the ligation state of the haem group.

Over the interparticle length scale, the mass transport of the proteins themselves is the most relevant process. The diffusion of proteins in solution is most commonly measured with dynamic light scattering[59], but high-resolution neutron spectroscopy provides a measure[60] of the short-time diffusion coefficient of the protein inside the first neighbour shell, even in systems of high concentrations, that is, 'crowded' systems[61]. This measurement enables a description of protein diffusion based on theories and methods borrowed from the colloid community, which have led to the discovery of dynamic clusters of proteins[60,62,63]. However, such structuring of a protein is not long lived, as small fluctuations can break this organization. Besides the fundamental value of the research, this line of work has important implications for the pharmaceutical industry because, although short lived, the clusters affect the solution viscosity[64], which is an important parameter for the administration of therapeutic proteins, such as monoclonal antibodies[65].

Lipids. Another area of relevance for NSE and backscattering techniques is the investigation of the dynamics of lipid systems. Although much of the neutron scattering work on these samples is structural, high-energy-resolution neutron spectroscopy has played an important part in characterizing both simple model membranes and ones with biologically relevant entities. Understanding the microscopic dynamics in the complex mixture of lipids that constitute biological membranes could be the key to understanding many of the cellular processes that are regulated by lipid–lipid, lipid–protein or protein–protein interactions. At an individual level, the localized motions of lipid chains and self-diffusion of lipid molecules throughout the hydrated environment are accessible with backscattering spectroscopy, enabling a detailed atomic-level description of different lipids and revealing fundamental effects that contribute to the phase behaviour. In a simple case, a comparison of saturated and unsaturated lipids shows that double bonds restrict the mobility of the chains and may explain the lower bending and compressibility moduli in unsaturated membranes[66]. Increasing in complexity, lipid membranes can undergo various, and sometimes sizeable and physiologically important, changes when small molecules or peptides are present. Examples include antimicrobial peptides[67], neurotoxic amyloid-β,36 melittin[68], the anaesthetic ethanol[69] or even cholesterol under pressure[70]. Furthermore, new insight into the role of rafts was obtained through NSE measurements of the lateral diffusion coefficients in a phase-separated lipid mixture. In agreement with structural and dynamical data from molecular dynamics simulations, the measurements indicate that rafts function as buffers of membrane properties and that a change in the complex lipid compositions in response to a variation in external parameters (such as temperature) may provide an advantageous stabilizing effect[71].

At the level of the collective dynamics of lipid membranes, which determine the elastic properties and have a fundamental role in processes such as endocytosis and exocytosis as well as cell fission and fusion, measurements on large unilamellar vesicles of phospholipids represent a simple but valuable model. Modelling of the elastic properties is often based on the Helfrich expression of the bending Hamiltonian[72], which has been used to derive an expression of the intermediate scattering function that can well describe the NSE experimental data[73]. Recent advances in the theoretical understanding of how the bending energy is dispersed through the intermonolayer friction[74] has led to a better interpretation of the results from NSE studies on the bending modulus of a phospholipid bilayer, resolving previous disagreements with the results from other techniques. Moreover, it was also shown that the thickness fluctuations (peristaltic motion) of a membrane can be directly accessed by NSE[75]. This motion can be related to the elastic and viscous properties of the membranes[76]. Thus, these theoretical and experimental efforts have led to a unifying picture that enables the extraction of the main elastic and viscous parameters of the membrane through NSE measurements[77]. This type of neutron study has been used to investigate the effect of different components in the membrane, such as various lipids[78–81], cholesterol[82], drugs[83], proteins[84–86] and nanoparticles[87,88].

Complex biological systems. More realistic biological systems, which are far from the simple dilute solution limit, are often multicomponent and require the collection of multiple datasets from various techniques, including QENS. Diffusion processes in real cellular environments, which are characteristically crowded, can reveal how nature has optimized the protein content for optimum oxygen transport in red blood cells[89] or simply provide information about the multiscale nature of the diffusion processes occurring in such concentrated systems[90,91]. The concept of 'in-cell neutron scattering' (that is, neutron scattering on living cells) was showcased and followed by work on living planarian flatworms[92], whose metabolism relies on molecular diffusion through the body. Measurable microscopic diffusivities were surprisingly well defined in such a complex system. Of more importance to human health, backscattering data have revealed intracellular water as a secondary target in the interaction of the drug cisplatin with human nucleated cells of invasive breast carcinoma; this finding has provided a new and innovative way to optimize the pharmacodynamics of anticancer agents for breast and bone cancers[49,93]. Backscattering spectroscopy has also proved to be a complementary tool to overcome the experimental limit of diffusion magnetic resonance imaging, which is used to diagnose different brain diseases, by extracting information about the heterogeneity and asymmetries in brain tissue from water diffusion dynamics[50]. Finally, similar methods to those mentioned above for NSE on large unilamellar vesicles have been used to investigate the elastic properties in living cell membranes[94].

It is important to remark here that given the complexity (multicomponent and hierarchical nature) of

many biological and soft matter systems, valuable insight requires the combined use of different scattering techniques and spectrometers, often including neutrons, X-rays and light, covering different areas of the space–time map (FIG. 1) as well as other measurements and the use of computer simulations.

Dynamics in disordered magnets

As a common magnet is cooled, one expects to observe long-range, static magnetic order (often ferromagnetic or antiferromagnetic) below a critical temperature. The Curie–Weiss temperature is a classical mean-field parameter that is indicative of the magnetic coupling within a material and provides an estimate of the freezing temperature. In these textbook magnets, investigations with traditional inelastic neutron scattering, such as three-axis spectrometers, working in energy space are making notable contributions to understanding the microscopic dynamics. Backscattering spectrometers are routinely used in the study of these magnets when low-energy excitations or small gaps in the excitation spectrum are expected, taking advantage of the very high resolution of the spectrometer[95]. However, for studies of more exotic magnets, such as those with quantum fluctuations or low dimensionality, high-resolution neutron spectroscopy is needed to simultaneously access the spatial and temporal correlations in the low μeV to meV range. Spin glasses, frustrated magnets and spin liquids all exhibit slow spin-relaxation phenomena and require a detailed measure of the spectral weight below 1 meV (see the example in FIG. 3a). We focus here on the impact of backscattering and NSE studies on geometrically frustrated magnets[96], but it should be noted that studies of magnetism have benefited from measurements using these instruments in many other areas of research, including spin glasses[97] and unconventional superconductors[98].

In a geometrically frustrated magnet, the spatial connections between magnetic ions are such that not all near-neighbour exchange bonds can be satisfied simultaneously[99–105]. An intuitive example is that of an Ising antiferromagnet on a triangular or Kagome lattice (FIG. 3c). A near 2D spin arrangement like this is realized in several materials and structure types, such as delafossite[102] or herbertsmithite[103]. Three-dimensional examples of lattices that invite geometrical frustration are the pyrochlore[104] (FIG. 3b) and garnet lattices[105].

One of the consequences of geometrical frustration is that these materials often have a high density of low-energy states, making them susceptible to low-energy (slow) fluctuations. In extreme cases, this macroscopic degeneracy of the ground state suppresses the expected ordering down to the lowest temperatures. Experimentally, it is observed that the material may still enter a long-range ordered state albeit at a much lower temperature[106]. Alternatively, a material may freeze into a spin-glass state, as observed for $Y_2Mo_2O_7$ (REF.[107]), or the spin system may stay dynamic down to the lowest temperature that is experimentally accessible and form a 'spin liquid'[108,109]. In the 2D, antiferromagnetically coupled triangular sublattice of $NiGa_2S_4$ (REF.[101]), more than 12 decades of relaxation time were probed (FIG. 3d) from room temperature down to 100 mK. A distinctive critical slowing down of the spin fluctuation was observed at ~8.5 K, but conventional long-range order was not found.

To date, it has been difficult to predict, from first principles alone, what happens to the spin ensemble of a frustrated magnet upon cooling. Fine details of the chemistry of the material may become important, such as site disorder or off-stoichiometry composition. This can occur even with ≤1% disorder or off-stoichiometry, which is hard to quantify by measurement. A case in point is $Yb_2Ti_2O_7$, a pyrochlore magnet very close to a ferromagnetic–antiferromagnetic phase boundary. Initial results, including high-resolution neutron scattering measurements, suggested the system was dynamic to 50 mK (REFS[110–112]), but it was later shown using neutron diffraction that it can also freeze, depending on minute chemical and crystallographic differences[113,114].

Spin ices[115] and related ferromagnetically frustrated magnets have illustrated the value of QENS for uncovering the underlying physics. The dynamic processes in these materials cover a wide dynamic range and become very slow at low temperature[116–119], which makes it nearly impossible to cool a crystal of spin ice below ~0.3 K because the relaxation times diverge and heat flow becomes increasingly slow[120].

The low-temperature neutron scattering signal of a classical spin ice features 'pinch points' in reciprocal space, for example, at the (002) and (111) positions[121]. These points result directly from long-range dipolar interactions and are now interpreted in terms of a 'Coulomb phase'. The dynamic dimension of this scattering was revealed in an NSE experiment[116] in which the relaxational spin dynamics above 5 K were observed to have four defining characteristics: first, the dynamics are unusually slow; second, only one timescale exists in the entire spin ensemble; third, the dynamics are independent of Q; and, last, they are thermally activated with a characteristic relaxation time of $\tau = \tau_0 \exp(T_K/T)$, with $\tau_0 \approx 4.5 \times 10^{-12}$ s and, for $Ho_2Ti_2O_7$, an activation temperature (T_K) of 293 K. These NSE results have been reproduced using a backscattering spectrometer[118], although the analysis was more difficult than that of the NSE data owing to the signal being close to the resolution of the spectrometer. This picture survives at temperatures well above room temperature, and more than two orders of magnitude above that of the spin ice or Coulomb phase, showing that spin ice is not a typical paramagnet even at room temperature. Upon cooling below 5 K, backscattering results and measurement of the dynamic susceptibility reveal a crossover in the relaxation rates with a decrease in the activation temperature to ~10 K. This crossover was first observed in 2004 and described as a mystery[117]. More recently, this low-temperature region has been modelled[121] as the relaxation phenomena associated with monopole creation, annihilation and propagation, which cost a few kelvin of energy.

In a related material, $Nd_2Zr_2O_7$ (REF.[122]), high-resolution inelastic scattering was needed to identify the various components of the scattering signal, and a 'moment fragmentation' model was introduced[123] to describe the coexistence of magnetic Bragg scattering and diffuse scattering.

Two local probes that are uniquely sensitive to slow magnetic fluctuations are muon spectroscopy and

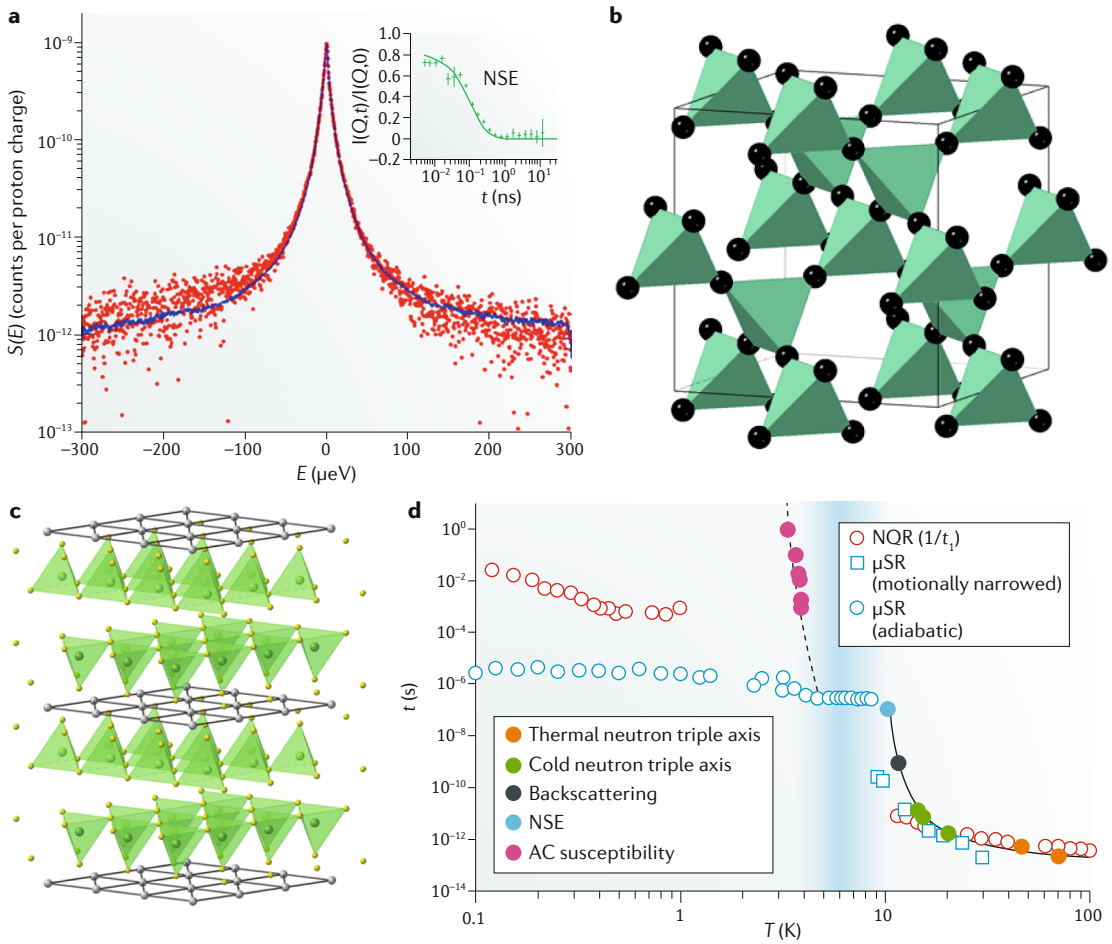

Fig. 3 | **Slow spin dynamics in disordered magnets. a,b** | Quasi-elastic broadening observed in a La-diluted spin ice using a backscattering spectrometer[100] (panel **a**) and by a neutron spin-echo (NSE) spectrometer (shown in the inset). Red points are original data points of the backscattering measurement. The blue line is the fit through the data calculated from a Lorentzian scattering law convoluted with the (experimentally determined) instrumental resolution. Error bars in the inset are calculated from the counting statistics of the spin-echo measurement. Here, the frustrated moments decorate a sublattice of corner-sharing tetrahedra (panel **b**). The measurements were performed under similar conditions and highlight the difference between working in energy space and measuring the dynamic structure factor ($S(E)$, where E is the energy transfer) and in time measuring the normalized intermediate scattering functions, here denoted as $I(Q,t)/I(Q,0)$ (where Q is the wavevector transfer and t is time). **c,d** | Muon spin relaxation (μSR) and nuclear quadrupole resonance (NQR) complement a series of neutron-based measurements, including backscattering and NSE, to elucidate the spin dynamics (panel **d**) of an antiferromagnetic triangular lattice of $NiGa_2S_4$ where nickel, gallium and sulfur are represented by grey, green and yellow spheres, respectively (panel **c**). More than 12 decades of relaxation time were probed, enabling important conclusions to be drawn from this unique spin system and revealing a crossover regime highlighted by the blue vertical band. T, temperature; t_1, longitudinal (or spin-lattice) relaxation time . Panel **a** is adapted with permission from REF.[100], Institute of Physics. Panel **d** is adapted with permission from REF.[101], American Physical Society.

Mössbauer spectroscopy, and data from these probes are often presented alongside data from high-energy resolution neutron spectroscopy. Local probes do not offer a spatial dimension to the relaxational dynamics, but these techniques have unique merits; for example, muon spectroscopy is sensitive to very slow low-amplitude fluctuations, whereas Mössbauer spectroscopy is element specific. Reports on the application of Mössbauer spectroscopy to geometrically frustrated magnets are sparse in the literature; however, unusually slow spin dynamics were observed in some pyrochlores[111,124]. By contrast, a substantial body of work has been carried out on spin ices using muon spectroscopy[124–127], but the interpretation of the data has often contradicted those from other techniques or has been controversial within the muon community.

Jamming and glassiness is observed in a wide variety of systems, including granular media, colloidal suspensions, molecular systems and magnets. These systems exhibit non-equilibrium transitions from a fluid-like to a solid-like state. Jamming of particles or spins, in local mimima of an exotic energy landscape, precludes further exploration of the phase space[128,129], but the characteristic sudden arrest of their dynamics are readily probed using NSE and backscattering techniques[130,131]. Glass transition, gelation and aggregation are all closely related and only the wide coverage of Q and energy space provided by these neutron techniques can help to distinguish

such dynamics[132]. Other probes, such as dynamic light scattering and photon correlation spectroscopy, offer complementary information to the results from neutron spectroscopy in these areas.

Finally, other studies of magnetism that have benefited from quasielastic scattering include those on vortex dynamics in type-II superconductors, dynamics of large topological structures such as skyrmions and unconventional intermetallic materials[98,133–135]. Extraordinary studies like these have been performed on magnetic systems, but at present, the experiments are not routine and models to interpret the data are limited.

Conclusion and outlook

The backscattering and NSE techniques uniquely provide spatial and temporal information on molecular and spin dynamics occurring in a space and time range from ~1 Å up to hundreds of nanometres and from tens of picoseconds to hundreds of nanoseconds, respectively. Backscattering and NSE spectrometers have unique strengths, such as the simultaneous access to the time and space domains, the sensitivity to isotopes (in particular, the contrast between hydrogen and deuterium) and the ability to study a material at extreme conditions of temperature. We have highlighted here research in polymers, biomolecules and disordered magnets; however, the study of the dynamics within liquids, molecular motions under nanoscopic confinement or on surfaces and diffusion of hydrogen in solid-state materials are also fields in which high-energy-resolution neutron spectroscopy techniques can provide relevant information[136,137]. Moreover, QENS can give quantitative insight into atomic-scale proton[138] and ionic conduction mechanisms in ionic liquids or solid electrolytes[139–141]. These instruments also have a role in the optimization of the thermodynamic stability, kinetics and reversibility of hydrogen storage in solid-state materials[142] and the dynamics of ions and molecules in green energy materials such as polymer-based batteries[30].

Although this Technical Review focuses on relaxational dynamics, high-resolution spectrometers can also probe truly inelastic features within the dynamic range of the spectrometer. These features include the tunnelling of methyl groups in soft matter[143], quantum tunnelling in molecules[144] and low-lying electronic spin excitations[145]. However, it would be remiss not to mention studies of the nuclear spin[146–148]. With energy transfers of <100 μeV and very weak signals, these studies are still time consuming and are only possible on the best backscattering spectrometers. However, future spectrometers will reduce the time required and/or an increase in the number of instruments that can probe such excitations will open up the possibility of studying these quantum effects with applications in, for example, quantum computing.

The intensity of the beams of cold neutrons (<5 meV) required for backscattering and NSE studies is increasing with the development of brighter sources and neutron transport systems. Modern instrumentation is continuously expanding the region of the space–time map covered by these spectrometers as well as increasing the data acquisition rate. These developments, together with those of the ancillary sample environment, are enabling these techniques to be used by an ever-broader user community in diverse research fields and providing complementary information on the relaxation processes (motions) to that available through other techniques, such as dielectric spectroscopy, NMR, muon spin relaxation, photon correlation spectroscopy and tracer diffusion measurements.

A notable breakthrough in backscattering instrumentation was the development of GaAs(200) analyser crystals[149]. At present, these crystals provide an energy resolution of 77 neV, an improvement of a factor of 10 over traditional Si(111) analyser crystals. However, the resolution is still far from the theoretical limit of 13.2 neV. Current developments aim to improve the Q resolution of backscattering spectrometers, widen the accessible energy transfer range (to enable dynamics to be probed over a wider range of timescales) and to deploy modern beam polarization techniques at these instruments. The latter will extend the capabilities of quasi-elastic neutron spectroscopy by providing a clean separation of coherent and incoherent scattering, enabling the isolation of weak magnetic signals or providing access to the directional components of the magnetization of a sample. The newest backscattering spectrometer, MIRACLES, will be built at the European Spallation Source (Sweden) and will give researchers greater flexibility in choosing between flux and resolution while also extending the dynamic range of backscattering spectrometers[150].

Recent developments at IN15 and J-NSE-Phoenix have increased the uniformity and magnitude of the precession fields, improving the energy resolution to beyond 1 neV. In parallel, the development of WASP aims to mitigate in some cases the severe limitation in the data acquisition rate of the technique by covering more of the Q space simultaneously. Furthermore, the development and implementation of resonant spin-echo methods will enable application to systems currently out of reach, namely samples that depolarize the neutron beam.

High-energy-resolution neutron spectroscopy studies have a unique role in understanding the dynamics of proteins and the water of hydration, lipid membranes and self-assembled amphiphilic structures. There is considerable potential in probing both the internal dynamics of lipids and the diffusion rates, developing on recent NSE work on the elastic and viscous properties of model membranes. QENS studies of hard matter would benefit tremendously from tools to handle single-crystal samples. Progress in this area will enable studies of anisotropic interactions, exotic magnetic phases, such as skyrmions and quantum spin liquids, and low-dimensional features such as stripe phases.

This Technical Review provides a glimpse of the future potential of NSE and backscattering spectrometers. In parallel with other methods, such as X-ray photon correlation spectroscopy and molecular dynamics simulations, these high-resolution neutron spectroscopic techniques will reveal new scientific phenomena. We hope this Technical Review provides readers with understanding of the potential of quasi-elastic neutron studies in their research.

Published online: 02 January 2020

1. Furrer, A., Mesot, J. & Strässle T. *Neutron Scattering in Condensed Matter Physics* (World Scientific, 2009).
2. Lovesey, S. W. *Theory of Neutron Scattering from Condensed Matter* (Clarendon Press, 1984).
3. Sears, V. F. Neutron scattering lengths and cross sections. *Neutron News* **3**, 26–37 (1992).
4. Bée, M. *Quasielastic Neutron Scattering: Principles and Applications in Solid State Chemistry, Biology and Materials Science* (A. Hilger, 1988).
5. Van Hove, L. Correlations in space and time and Born approximation scattering in systems of interacting particles. *Phys. Rev.* **95**, 249–262 (1954).
6. Ehlers, G. Study of slow dynamic processes in magnetic systems by neutron spin-echo spectroscopy. *J. Phys. Condens. Matter* **18**, R231 (2006).
7. Richter, D., Monkenbusch, M., Arbe A. & Colmenero, J. *Neutron Spin Echo in Polymer Systems* (Springer, 2005).
8. Tyagi, M. & Chathoth, S. M. in *X-ray and Neutron Techniques for Nanomaterials Characterization* Ch. 14 (ed. Kumar, C.) 761–813 (Springer, 2016).
9. Frick, B. *Neutron Backscattering Spectroscopy* (Springer, 2006).
10. Hoffmann, I. Neutrons for the study of dynamics in soft matter systems. *Colloid Polym. Sci.* **292**, 2053–2069 (2014).
11. Ohl, M. et al. The spin-echo spectrometer at the Spallation Neutron Source (SNS). *Nucl. Instrum. Methods Phys. Res. A* **696**, 85–99 (2012).
12. Seto, H. et al. Inelastic and quasi-elastic neutron scattering spectrometers in J-PARC. *Biochim. Biophys. Acta Gen. Sub.* **1861**, 3651–3660 (2017).
13. Schmidt, C. J., Groitl, F., Klein, M., Schmidt, U. & Häussler, W. CASCADE with NRSE: fast intensity modulation techniques used in quasielastic neutron scattering. *J. Phys. Conf. Ser.* **251**, 012067 (2010).
14. Pasini, S. & Monkenbusch, M. Optimized superconducting coils for a high-resolution neutron spin-echo spectrometer at the European Spallation Source, ESS. *Meas. Sci. Technol.* **26**, 035501 (2015).
15. Farago, B. et al. The IN15 upgrade. *Neutron News* **26**, 15–17 (2015).
16. Ivanova, O., Pasini, S., Monkenbusch, M. & Holderer, O. Instrument developments and recent scientific highlights at the J-NSE. *J. Phys. Conf. Ser.* **862**, 012009 (2017).
17. Hong, L., Smolin, N. & Smith, J. C. De Gennes narrowing describes the relative motion of protein domains. *Phys. Rev. Lett.* **112**, 158102 (2014).
18. Pappas, C., Kischnik, R. & Mezei, F. Wide angle NSE: the spectrometer SPAN at BENSC. *Physica B* **297**, 14–17 (2001).
19. Fouquet, P., Ehlers, G., Farago, B., Pappas, C. & Mezei, F. The wide-angle neutron spin echo spectrometer project WASP. *J. Neutron Res.* **15**, 39–47 (2007).
20. Frick, B., Mamontov, E., van Ejick, L. & Seydel, T. Recent backscattering instrument developments at the ILL and SNS. *Z. Phys. Chem.* **224**, 33–60 (2010).
21. Francesca, N. et al. IN13 backscattering spectrometer at ILL: looking for motions in biological macromolecules and organisms. *Neutron News* **19**, 14–18 (2008).
22. Mamontov, E. & Herwig, K. W. A time-of-flight backscattering spectrometer at the Spallation Neutron Source, BASIS. *Rev. Sci. Instrum.* **82**, 085109 (2011).
23. Demmel, F. et al. ToF-backscattering spectroscopy at the ISIS facility: status and perspectives. *J. Phys. Conf. Ser.* **1021**, 012027 (2018).
24. Telling, M. T. F. & Andersen, K. H. Spectroscopic characteristics of the OSIRIS near-backscattering crystal spectrometer on the ISIS pulsed neutron source. *Phys. Chem. Chem. Phys.* **7**, 1255–1261 (2004).
25. Appel, M., Frick, B. & Magerl, A. A flexible high speed pulse chopper system for an inverted neutron time-of-flight option on backscattering spectrometers. *Sci. Rep.* **8**, 13580 (2018).
26. Lautner, L. et al. Dynamic processes in biological membrane mimics revealed by quasielastic neutron scattering. *Chem. Phys. Lipids* **206**, 28–42 (2017).
27. Monkenbusch, M., Richter, D. & Biehl, R. Observation of protein domain motions by neutron spectroscopy. *ChemPhysChem* **11**, 1188–1194 (2010).
28. de Gennes, P. G. Quasi-elastic scattering of neutrons by dilute polymer solutions: I. Free-draining limit. *Phys. Phys. Fiz.* **3**, 37–45 (1967).
29. Higgins, J. S. & Benoît, H. *Polymers and Neutron Scattering* (Oxford Univ. Press, 1994).
30. Mongcopa, K. I. S. et al. Relationship between segmental dynamics measured by quasi-elastic neutron scattering and conductivity in polymer electrolytes. *ACS Macro Lett.* **7**, 504–508 (2018).
31. Ateyyah, M. et al. Temperature-dependent structure and dynamics of highly-branched poly(*N*-isopropylacrylamide) in aqueous solution. *Soft Matter* **14**, 1482–1491 (2018).
32. Sakai, V. G. & Arbe, A. Quasielastic neutron scattering in soft matter. *Curr. Opin. Colloid Interface Sci.* **14**, 381–390 (2009).
33. Schneider, G. J., Nusser, K., Willner, L., Falus, P. & Richter, D. Dynamics of entangled chains in polymer nanocomposites. *Macromolecules* **44**, 5857–5860 (2011).
34. Glomann, T. et al. Microscopic dynamics of polyethylene glycol chains interacting with silica nanoparticles. *Phys. Rev. Lett.* **110**, 178001 (2013).
35. Senses, E., Faraone, A. & Akcora, P. Microscopic chain motion in polymer nanocomposites with dynamically asymmetric interphases. *Sci. Rep.* **6**, 29326 (2016).
36. Senses, E., Tyagi, M., Pasco, M. & Faraone, A. Dynamics of architecturally engineered all-polymer nanocomposites. *ACS Nano* **12**, 10807–10816 (2018).
37. Arbe, A. et al. Single chain dynamic structure factor of linear polymers in an all-polymer nano-composite. *Macromolecules* **49**, 2354–2364 (2016).
38. Monkenbusch, M. et al. Molecular view on supramolecular chain and association dynamics. *Phys. Rev. Lett.* **117**, 147802 (2016).
39. Krutyeva, M. et al. Effect of nanoconfinement on polymer dynamics: surface layers and interphases. *Phys. Rev. Lett.* **110**, 108303 (2013).
40. Krutyeva, M. et al. Polymer dynamics under cylindrical confinement featuring a locally repulsive surface: a quasielastic neutron scattering study. *J. Chem. Phys.* **146**, 203306 (2017).
41. Li, Y., Kroger, M. & Liu, W. K. Nanoparticle effect on the dynamics of polymer chains and their entanglement network. *Phys. Rev. Lett.* **109**, 118001 (2012).
42. Senses, E. et al. Small particle driven chain disentanglements in polymer nanocomposites. *Phys. Rev. Lett.* **118**, 147801 (2017).
43. Doster, W., Cusack, S. & Petry, W. Dynamical transition of myoglobin revealed by inelastic neutron scattering. *Nature* **337**, 754–756 (1989).
44. Benedetto, A. Low-temperature decoupling of water and protein dynamics measured by neutron scattering. *J. Phys. Chem. Lett.* **8**, 4883–4886 (2017).
45. Tehei, M. et al. Adaptation to extreme environments: macromolecular dynamics in bacteria compared in vivo by neutron scattering. *EMBO Rep.* **5**, 66–70 (2004).
46. Librizzi, F., Carrotta, R., Peters, J. & Cupane, A. The effects of pressure on the energy landscape of proteins. *Sci. Rep.* **8**, 2037 (2018).
47. Zaccai, G. et al. Neutrons describe ectoine effects on water H-bonding and hydration around a soluble protein and a cell membrane. *Sci. Rep.* **6**, 31434 (2016).
48. Liu, Z. et al. Entropic contribution to enhanced thermal stability in the thermostable P450 CYP119. *Proc. Natl Acad. Sci. USA* **115**, E10049–E10058 (2018).
49. Marques, M. P. M. et al. Intracellular water — an overlooked drug target? Cisplatin impact in cancer cells probed by neutrons. *Phys. Chem. Chem. Phys.* **19**, 2702–2713 (2017).
50. Natali, F. et al. Water dynamics in neural tissue. *J. Phys. Soc. Jpn* **82**, SA017 (2013).
51. Stingaciu, L. R., Ivanova, O., Ohl, M., Biehl, R. & Richter, D. Fast antibody fragment motion: flexible linkers act as entropic spring. *Sci. Rep.* **6**, 22148 (2016).
52. Stadler, A. M. et al. Internal nanosecond dynamics in the intrinsically disordered myelin basic protein. *J. Am. Chem. Soc.* **136**, 6987–6994 (2014).
53. Ameseder, F. et al. Relevance of internal friction and structural constraints for the dynamics of denatured bovine serum albumin. *J. Phys. Chem. Lett.* **9**, 2469–2473 (2018).
54. Callaway, D. J. E. & Bu, Z. M. Visualizing the nanoscale: protein internal dynamics and neutron spin echo spectroscopy. *Curr. Opin. Struct. Biol.* **42**, 1–5 (2017).
55. Biehl, R., Monkenbusch, M. & Richter, D. Exploring internal protein dynamics by neutron spin echo spectroscopy. *Soft Matter* **7**, 1299–1307 (2011).
56. Hong, L. et al. Structure and dynamics of a compact state of a multidomain protein, the mercuric ion reductase. *Biophys. J.* **107**, 393–400 (2014).
57. Hong, L. et al. Determination of functional collective motions in a protein at atomic resolution using coherent neutron scattering. *Sci. Adv.* **2**, e1600886 (2016).
58. Fujiwara, S. et al. Ligation-dependent picosecond dynamics in human hemoglobin as revealed by quasielastic neutron scattering. *J. Phys. Chem. B* **121**, 8069–8077 (2017).
59. Berne, B. J. & Pecora, R. *Dynamic Light Scattering: With Applications to Chemistry, Biology, and Physics* (Dover Publications, 2000).
60. Porcar, L. et al. Formation of the dynamic clusters in concentrated lysozyme protein solutions. *J. Phys. Chem. Lett.* **1**, 126–129 (2010).
61. Bucciarelli, S. et al. Dramatic influence of patchy attractions on short-time protein diffusion under crowded conditions. *Sci. Adv.* **2**, e1601432 (2016).
62. Godfrin, P. D. et al. Dynamic properties of different liquid states in systems with competing interactions studied with lysozyme solutions. *Soft Matter* **14**, 8570–8579 (2018).
63. Riest, J., Nagele, G., Liu, Y., Wagner, N. J. & Godfrin, P. D. Short-time dynamics of lysozyme solutions with competing short-range attraction and long-range repulsion: experiment and theory. *J. Chem. Phys.* **148**, 065101 (2018).
64. Dharmaraj, V. L., Godfrin, P. D., Liu, Y. & Hudson, S. D. Rheology of clustering protein solutions. *Biomicrofluidics* **10**, 043509 (2016).
65. Godfrin, P. D. et al. Effect of hierarchical cluster formation on the viscosity of concentrated monoclonal antibody formulations studied by neutron scattering. *J. Phys. Chem. B* **120**, 278–291 (2016).
66. Nanda, H. et al. Relaxation dynamics of saturated and unsaturated oriented lipid bilayers. *Soft Matter* **14**, 6119–6127 (2018).
67. Sharma, V. K., Mamontov, E., Anunciado, D. B., O'Neill, H. & Urban, V. S. Effect of antimicrobial peptide on the dynamics of phosphocholine membrane: role of cholesterol and physical state of bilayer. *Soft Matter* **11**, 6755–6767 (2015).
68. Buck, Z. N. et al. Effect of melittin on water diffusion and membrane structure in DMPC lipid bilayers. *Europhys. Lett.* **123**, 18002 (2018).
69. Toppozini, L. et al. Partitioning of ethanol into lipid membranes and its effect on fluidity and permeability as seen by X-ray and neutron scattering. *Soft Matter* **8**, 11839–11849 (2012).
70. Peters, J. et al. Thermodynamics of lipid multi-lamellar vesicles in presence of sterols at high hydrostatic pressure. *Sci. Rep.* **7**, 15339 (2017).
71. Nickels, J. D. et al. Lipid rafts: buffers of cell membrane physical properties. *J. Phys. Chem. B* **123**, 2050–2056 (2019).
72. Helfrich, W. Elastic properties of lipid bilayers: theory and possible experiments. *Z. Naturforsch. C* **28**, 693–703 (1973).
73. Zilman, A. G. & Granek, R. Undulations and dynamic structure factor of membranes. *Phys. Rev. Lett.* **77**, 4788–4791 (1996).
74. Watson, M. C. & Brown, F. L. H. Interpreting membrane scattering experiments at the mesoscale: the contribution of dissipation within the bilayer. *Biophys. J.* **98**, L9–L11 (2010).
75. Woodka, A. C., Butler, P. D., Porcar, L., Farago, B. & Nagao, M. Lipid bilayers and membrane dynamics: insight into thickness fluctuations. *Phys. Rev. Lett.* **109**, 058102 (2012).
76. Bingham, R. J., Smye, S. W. & Olmsted, P. D. Dynamics of an asymmetric bilayer lipid membrane in a viscous solvent. *Europhys. Lett.* **111**, 18004 (2015).
77. Nagao, M., Kelley, E. G., Ashkar, R., Bradbury, R. & Butler, P. D. Probing elastic and viscous properties of phospholipid bilayers using neutron spin echo spectroscopy. *J. Phys. Chem. Lett.* **8**, 4679–4684 (2017).
78. Pan, J. et al. Structural and mechanical properties of cardiolipin lipid bilayers determined using neutron spin echo, small angle neutron and X-ray scattering, and molecular dynamics simulations. *Soft Matter* **11**, 130–138 (2015).
79. Ashkar, R. et al. Tuning membrane thickness fluctuations in model lipid bilayers. *Biophys. J.* **109**, 106–112 (2015).
80. Nickels, J. D. et al. Mechanical properties of nanoscopic lipid domains. *J. Am. Chem. Soc.* **137**, 15772–15780 (2015).
81. Nickels, J. D. et al. *Bacillus subtilis* lipid extract, a branched-chain fatty acid membrane model. *J. Phys. Chem. Lett.* **8**, 4214–4217 (2017).
82. Bruning, B. A. et al. Bilayer undulation dynamics in unilamellar phospholipid vesicles: effect of temperature, cholesterol and trehalose. *Biochim. Biophys. Acta Biomembr.* **1838**, 2412–2419 (2014).
83. Yi, Z., Nagao, M. & Bossev, D. P. Effect of charged lidocaine on static and dynamic properties of model bio-membranes. *Biophys. Chem.* **160**, 20–27 (2012).
84. Heller, W. T. & Zolnierczuk, P. A. The helix-to-sheet transition of an HIV-1 fusion peptide derivative changes the mechanical properties of lipid bilayer membranes. *Biochim. Biophys. Acta Biomembr.* **1861**, 565–572 (2019).

85. Lee, J.-H. et al. Thermal fluctuation and elasticity of lipid vesicles interacting with pore-forming peptides. *Phys. Rev. Lett.* **105**, 038101 (2010).
86. Sreij, R. et al. DMPC vesicle structure and dynamics in the presence of low amounts of the saponin aescin. *Phys. Chem. Chem. Phys.* **20**, 9070–9083 (2018).
87. Chakraborty, S., Abbasi, A., Bothun, G. D., Nagao, M. & Kitchens, C. L. Phospholipid bilayer softening due to hydrophobic gold nanoparticle inclusions. *Langmuir* **34**, 13416–13425 (2018).
88. Hoffmann, I. et al. Softening of phospholipid membranes by the adhesion of silica nanoparticles — as seen by neutron spin-echo (NSE). *Nanoscale* **6**, 6945–6952 (2014).
89. Longeville, S. & Stingaciu, L. R. Hemoglobin diffusion and the dynamics of oxygen capture by red blood cells. *Sci. Rep.* **7**, 10448 (2017).
90. Braun, M. K. et al. Crowding-controlled cluster size in concentrated aqueous protein solutions: structure, self- and collective diffusion. *J. Phys. Chem. Lett.* **8**, 2590–2596 (2017).
91. Anunciado, D. B. et al. In vivo protein dynamics on the nanometer length scale and nanosecond time scale. *J. Phys. Chem. Lett.* **8**, 1899–1904 (2017).
92. Mamontov, E. Microscopic diffusion processes measured in living planarians. *Sci. Rep.* **8**, 4190 (2018).
93. Marques, M. P. M. et al. Chemotherapeutic targets in osteosarcoma — insights from synchrotron-MicroFTIR and quasi-elastic neutron scattering. *J. Phys. Chem. B* **123**, 6968–6979 (2019).
94. Stingaciu, L. R. et al. Revealing the dynamics of thylakoid membranes in living cyanobacterial cells. *Sci. Rep.* **6**, 19627 (2016).
95. Stock, C. et al. Solitary magnons in the $S=5/2$ antiferromagnet $CaFe_2O_4$. *Phys. Rev. Lett.* **117**, 017201 (2016).
96. Zvyagin, A. A. New physics in frustrated magnets: spin ices, monopoles, etc. (Review Article). *Low. Temp. Phys.* **39**, 901–922 (2013).
97. Mydosh, J. A. Spin glasses: redux: an updated experimental/materials survey. *Rep. Prog. Phys.* **78**, 052501 (2015).
98. Blackburn, E. et al. Fermi surface topology and the superconducting gap function in UPd_2Al_3: a neutron spin-echo study. *Phys. Rev. Lett.* **97**, 057002 (2006).
99. Starykh, O. A. Unusual ordered phases of highly frustrated magnets: a review. *Rep. Prog. Phys.* **78**, 052502 (2015).
100. Ehlers, G. et al. Frustrated spin correlations in diluted spin ice $Ho_{2-x}La_xTi_2O_7$. *J. Phys. Condens. Matter* **20**, 235206 (2008).
101. Nambu, Y. et al. Spin fluctuations from hertz to terahertz on a triangular lattice. *Phys. Rev. Lett.* **115**, 127202 (2015).
102. Ye, F. et al. Spontaneous spin-lattice coupling in the geometrically frustrated triangular lattice antiferromagnet $CuFeO_2$. *Phys. Rev. B* **73**, 220404 (2006).
103. Norman, M. R. Herbertsmithite and the search for the quantum spin liquid. *Rev. Mod. Phys.* **88**, 041002 (2016).
104. Gardner, J. S., Gingras, M. J. P. & Greedan, J. E. Magnetic pyrochlore oxides. *Rev. Mod. Phys.* **82**, 52–107 (2010).
105. Paddison, J. A. M. et al. Hidden order in spin-liquid $Gd_3Ga_5O_{12}$. *Science* **350**, 179–181 (2015).
106. Lee, S.-H. et al. Emergent excitations in a geometrically frustrated magnet. *Nature* **418**, 856–858 (2002).
107. Gardner, J. S. et al. Glassy statics and dynamics in the chemically ordered pyrochlore antiferromagnet $Y_2Mo_2O_7$. *Phys. Rev. Lett.* **83**, 211–214 (1999).
108. Balents, L. Spin liquids in frustrated magnets. *Nature* **464**, 199–208 (2010).
109. Paddison, J. et al. Continuous excitations of the triangular-lattice quantum spin liquid $YbMgGaO_4$. *Nat. Phys.* **13**, 117–122 (2017).
110. Yasui, Y. et al. Ferromagnetic transition of pyrochlore compound $Yb_2Ti_2O_7$. *J. Phys. Soc. Jpn* **72**, 3014–3015 (2003).
111. Hodges, J. A. et al. First order transition in the spin dynamics of geometrically frustrated $Yb_2Ti_2O_7$. *Phys. Rev. Lett.* **88**, 077204 (2002).
112. Gardner, J. S., Ehlers, G., Rosov, N., Erwin, R. W. & Petrovic, C. Spin-spin correlations in $Yb_2Ti_2O_7$: a polarized neutron scattering study. *Phys. Rev. B* **70**, 180404(R) (2004).
113. Peçanha-Antonio, V. et al. Magnetic excitations in the ground state of $Yb_2Ti_2O_7$. *Phys. Rev. B* **96**, 214415 (2017).
114. Ross, K. A. et al. Lightly stuffed pyrochlore structure of single-crystalline $Yb_2Ti_2O_7$ grown by the optical floating zone technique. *Phys. Rev. B* **86**, 174424 (2012).
115. Bramwell, S. T. & Gingras, M. J. P. Spin ice state in frustrated magnetic pyrochlore materials. *Science* **294**, 1495–1501 (2001).
116. Ehlers, G. et al. Dynamical crossover in 'hot' spin ice. *J. Phys. Condens. Matter* **15**, L9 (2003).
117. Snyder, J. et al. Low-temperature spin freezing in the $Dy_2Ti_2O_7$ spin ice. *Phys. Rev. B* **69**, 064414 (2004).
118. Clancy, J. et al. Revisiting static and dynamic spin-ice correlations in $Ho_2Ti_2O_7$ with neutron scattering. *Phys. Rev. B* **79**, 014408 (2009).
119. Paulsen, C. et al. Far-from-equilibrium monopole dynamics in spin ice. *Nat. Phys.* **10**, 135–139 (2014).
120. Pomaranski, D. et al. Absence of Pauling's residual entropy in thermally equilibrated $Dy_2Ti_2O_7$. *Nat. Phys.* **9**, 353–356 (2013).
121. Jaubert, L. D. C. & Holdsworth, P. C. W. Magnetic monopole dynamics in spin ice. *J. Phys. Condens. Matter* **23**, 164222 (2011).
122. Petit, S. et al. Observation of magnetic fragmentation in spin ice. *Nat. Phys.* **12**, 746–750 (2016).
123. Brooks-Bartlett, M. E., Banks, S. T., Jaubert, L. D. C., Harman-Clarke, A. & Holdsworth, P. C. W. Magnetic-moment fragmentation and monopole crystallization. *Phys. Rev. X* **4**, 011007 (2014).
124. Snee, T. J., Meads, R. E. & Parker, W. G. A study of supertransferred hyperfine magnetic fields and relaxation of Dy^{3+} ions by Mössbauer spectroscopy of ^{57}Fe and $^{119}Sn^m$ in the pyrochlores $Dy_2Sn_2O_7$ and Dy_2FeSbO_7. *J. Phys. C* **10**, 1761–1773 (1977).
125. Bramwell, S. T. et al. Measurement of the charge and current of magnetic monopoles in spin ice. *Nature* **461**, 956–959 (2009).
126. Dunsiger, S. R. et al. Spin ice: magnetic excitations without monopole signatures using muon spin rotation. *Phys. Rev. Lett.* **107**, 207207 (2011).
127. Blundell, S. J. Monopoles, magnetricity, and the stray field from spin ice. *Phys. Rev. Lett.* **108**, 147601 (2012).
128. Edwards S. F. & Grinev, D. G. in *Jamming and Rheology: Constraint Dynamics on Microscopic and Macroscopic Scales* (eds Liu, A.J. & Nagel, S. R.) 80–93 (CRC Press, 2001).
129. Trappe, V., Prasad, V., Cipeletti, L., Segre, P. N. & Weltz, D. A. Jamming phase diagram for attractive particles. *Nature* **411**, 772–775 (2001).
130. Samarakoon, A. et al. Aging, memory, and nonhierarchical energy landscape of spin jam. *Proc. Natl Acad. Sci. USA* **113**, 11806–11810 (2016).
131. Samarakoon, A. M. et al. Scaling of memories and crossover in glassy magnets. *Sci. Rep.* **7**, 12053 (2017).
132. Pickup, R. M., Cywinski, R., Pappas, C., Farago, B. & Fouquet, P. Generalized spin-glass relaxation. *Phys. Rev. Lett.* **102**, 097202 (2009).
133. Forgan, E. M. et al. Measurement of vortex motion in a type-II superconductor: a novel use of the neutron spin-echo technique. *Phys. Rev. Lett.* **85**, 3488–3491 (2000).
134. Pappas, C. et al. Skyrmion lattice correlations. *Phys. Rev. Lett.* **119**, 047203 (2017).
135. Ehlers, G., Casalta, H., Lechner, R. E. & Maletta, H. Dynamics of frustrated magnetic moments in antiferromagnetically ordered TbNiAl probed by neutron time-of-flight and spin-echo spectroscopy. *Phys. Rev. B* **63**, 224407 (2001).
136. Hempelmann, R. *Quasielastic Neutron Scattering and Solid State Diffusion* (Oxford Univ. Press, 2000).
137. Karlsson, M. Perspectives of neutron scattering on proton conducting oxides. *Dalton Trans.* **42**, 317–329 (2013).
138. Karlsson, M. et al. Using neutron spin-echo to investigate proton dynamics in proton-conducting perovskites. *Chem. Mater.* **22**, 740–742 (2010).
139. Nemoto, F. et al. Neutron scattering studies on short- and long-range layer structures and related dynamics in imidazolium-based ionic liquids. *J. Chem. Phys.* **149**, 054502 (2018).
140. Berrod, Q. et al. Ionic liquids: evidence of the viscosity scale-dependence. *Sci. Rep.* **7**, 2241 (2017).
141. Lefevr, J., Cervini, L., Griffin, J. M. & Blanchard, D. Lithium conductivity and ions dynamics in $LiBH_4/SiO_2$ solid electrolytes studied by solid-state NMR and quasi-elastic neutron scattering and applied in lithium sulfur batteries. *J. Phys. Chem. C* **122**, 15264–15275 (2018).
142. Silvi, L. et al. A quasielastic and inelastic neutron scattering study of the alkaline and alkaline-earth borohydrides $LiBH_4$ and $Mg(BH_4)_2$ and the mixture $LiBH_4+Mg(BH_4)$. *Phys. Chem. Chem. Phys.* **21**, 718–728 (2019).
143. Do, C. et al. Methyl quantum tunneling in ionic liquid [DMIm][TFSI] facilitated by bis(trifluoromethane) sulfonimide lithium salt. *Sci. Rep.* **8**, 10354 (2018).
144. Canto, L. F., Gomes, P. R. S., Donangelo, R., Lubian, J. & Hussein, M. S. Recent developments in fusion and direct reactions with weakly bound nuclei. *Phys. Rep.* **596**, 1–86 (2015).
145. Thompson, J. D. et al. Quasiparticle breakdown and spin Hamiltonian of the frustrated quantum pyrochlore $Yb_2Ti_2O_7$ in a magnetic field. *Phys. Rev. Lett.* **119**, 057203 (2017).
146. Ehlers, G., Mamontov, E., Zamponi, M., Kam, K. C. & Gardner, J. S. Direct observation of a nuclear spin excitation in $Ho_2Ti_2O_7$. *Phys. Rev. Lett.* **102**, 016405 (2009).
147. Chatterji, T. & Frick, B. Nuclear spin excitations in $NdCu_2$. *Physica B* **350**, E111–E114 (2004).
148. Heidemann, A. Hyperfine interaction in amorphous ferromagnetic cobalt-phosphorous-alloys measured by inelastic neutron scattering. *Z. Phys. B* **20**, 385–389 (1975).
149. Kuhlmann, K., Appel, M., Frick, B. & Magerl, A. Breakthrough in neutron backscattering spectroscopy: energy resolution improved by one order of magnitude using the GaAs 200 reflection. *Rev. Sci. Instr.* **90**, 015119 (2019).
150. Tsapatsaris, N., Willendrup, P. K., Lechner, R. E. & Bordallo, H. N. From BASIS to MIRACLES: benchmarking and perspectives for high-resolution neutron spectroscopy at the ESS. *EPJ Web Conf.* **83**, 03015 (2015).
151. Mezei, F., Pappas, C. & Gutberlet T. (eds) *Neutron Spin Echo Spectroscopy* (Springer, 2003).
152. Mezei, F. (ed.) *Neutron Spin Echo* (Springer, 1979).
153. Niedzwiedz, K. et al. Chain dynamics and viscoelastic properties of poly(ethylene oxide). *Macromolecules* **41**, 4866–4872 (2008).
154. de Gennes, P. G. Reptation of a polymer chain in the presence of fixed obstacles. *J. Chem. Phys.* **55**, 572–579 (1971).
155. Farago, B. IN11C, medium-resolution multidetector extension of the IN11 NSE spectrometer at the ILL. *Physica B* **241–243**, 113–116 (1997).
156. Rosov, N., Rathgeber, S. & Monkenbusch, M. in *Scattering from Polymers: Characterization by X-Rays, Neutrons, and Light* Ch. 7 (Oxford Univ. Press, 2000).
157. Longeville, S. La spectroscopie neutronique à écho de spin à champ nul ou par résonance. *J. Phys. IV* **10**, 59–75 (2000).
158. Nagao, M. et al. Relocation and upgrade of neutron spin echo spectrometer, iNSE. *Physica B* **385–386**, 1118–1121 (2006).
159. Wuttke, J. et al. SPHERES, Jülich's high-flux neutron backscattering spectrometer at FRM II. *Rev. Sci. Instrum.* **83**, 075109 (2012).
160. Klose, F., Constantine, P., Kennedy, S. J. & Robinson, R. A. The Neutron Beam Expansion Program at the Bragg Institute. *J. Phys. Conf. Ser.* **528**, 012026 (2014).
161. Meyer, A., Dimeo, R. M., Gehring, P. M. & Neumann, D. A. The high-flux backscattering spectrometer at the NIST Center for Neutron Research. *Rev. Sci. Instrum.* **74**, 2759–2777 (2003).

Acknowledgements
The authors thank E. Senses and M. Nagao for critical reading of the manuscript, QENS instrument scientists worldwide and the research community, who keep bringing new research and challenges to the facilities. A.F. acknowledges support from the Center for High Resolution Neutron Scattering, a partnership between the National Institute of Standards and Technology and the US National Science Foundation under agreement no. DMR-1508249. This research used resources at the Spallation Neutron Source, a US Department of Energy Office of Science User Facility operated by the Oak Ridge National Laboratory. The authors thank J. Hemman, Oak Ridge National Laboratory Graphics Design Group, for support with some of the figures.

Author contributions
The authors contributed equally to all aspects of the article.

Competing interests
The authors declare no competing interests.

Peer review information
Nature Reviews Physics thanks A. Jackson and the other, anonymous, reviewer(s) for their contribution to the peer review of this work.

Supplementary information
Supplementary information is available for this paper at https://doi.org/10.1038/s42254-019-0128-1.